Cancer Research

# JARID1B Enables Transit between Distinct States of the Stem-like Cell Population in Oral Cancers

Nicole D. Facompre[1], Kayla M. Harmeyer[1], Xavier Sole[2], Sheheryar Kabraji[2], Zachary Belden[1], Varun Sahu[1], Kelly Whelan[3], Koji Tanaka[3], Gregory S. Weinstein[1], Kathleen T. Montone[4], Alexander Roesch[5], Phyllis A. Gimotty[6], Meenhard Herlyn[7], Anil K. Rustgi[3], Hiroshi Nakagawa[3], Sridhar Ramaswamy[2], and Devraj Basu[1,7,8]

## Abstract

The degree of heterogeneity among cancer stem cells (CSC) remains ill-defined and may hinder effective anti-CSC therapy. Evaluation of oral cancers for such heterogeneity identified two compartments within the CSC pool. One compartment was detected using a reporter for expression of the H3K4me3 demethylase JARID1B to isolate a JARID1B$^{high}$ fraction of cells with stem cell–like function. JARID1B$^{high}$ cells expressed oral CSC markers including CD44 and ALDH1 and showed increased PI3K pathway activation. They were distinguished from a fraction in a $G_0$-like cell-cycle state characterized by low reactive oxygen species and suppressed PI3K/AKT signaling. $G_0$-like cells lacked conventional CSC markers but were primed to acquire stem cell–like function by upregulating JARID1B, which directly mediated transition to a state expressing known oral CSC markers. The transition was regulated by PI3K signals acting upstream of JARID1B expression, resulting in PI3K inhibition depleting JARID1B$^{high}$ cells but expanding the $G_0$-like subset. These findings define a novel developmental relationship between two cell phenotypes that may jointly contribute to CSC maintenance. Expansion of the $G_0$-like subset during targeted depletion of JARID1B$^{high}$ cells implicates it as a candidate therapeutic target within the oral CSC pool. *Cancer Res; 76(18); 5538–49. ©2016 AACR.*



## Introduction

Cancer stem cells (CSC) are defined by unlimited self-renewal and differentiation to states lacking growth potential. They have been isolated in oral squamous cell carcinomas (OSCC) using multiple markers including CD44 and ALDH1 (1–3) and express regulators of embryonic stem cells including Oct4, Sox2, Nanog, and Bmi-1 (4–6). However, epigenetic plasticity among CSCs may prevent assignment of a single discrete molecular profile. Such plasticity among adult epithelial stem cells gives rise to quiescent and proliferative subsets that interconvert to support tissue homeostasis and repair (7, 8). Thus, similar heterogeneity among oral CSCs may drive cancer progression and shape therapy responses.

Although quiescence is not an essential stem cell trait, it is commonly attributed to adult stem cells and CSCs, where it may underlie generalized resistance to therapies targeting proliferating cells. As such, quiescence is defined by exit from the cell cycle while retaining cell division potential. One approach to defining quiescent cancer cells uses Pyronin-Y staining to gate cells with low total RNA within the $G_0$–$G_1$ fraction. Such cells exhibit the high p27$^{kip1}$ and low reactive oxygen species (ROS) of the $G_0$ state (9, 10). A related breast cancer subpopulation was isolated on the basis of low ROS and exhibits quiescent features including suppression of proliferation markers and increased Hes1 (11), an inhibitor of senescence and differentiation (12). Not meeting strict criteria for complete $G_0$ exit, these "$G_0$-like" cells downregulate PI3K/Akt signaling through proteasome-mediated Akt degradation (11, 13). The role of PI3K/Akt activation in allowing certain adult stem cells to exit quiescence (14) suggests that the pathway might also permit $G_0$-like cells to exert CSC function.

However, some molecular traits of $G_0$-like cells diverge from those described for CSCs, making their relationship unclear. Specifically, PI3K activation observed in putative CSCs of various cancers renders them sensitive to PI3K inhibitors (15–18). Furthermore, the ROS$^{low}$ feature of $G_0$-like cells is incongruous with the high oxidative metabolism observed in melanoma CSCs that express increased levels of the H3K4me3 demethylase JARID1B (19). These JARID1B$^{high}$ melanoma cells are slow-cycling (20) but are not known to express markers of quiescence. JARID1B, a transcriptional repressor, targets genes involved in diverse cellular processes including development, differentiation, and cell cycle (21–23). It is overexpressed in various cancers (23–25). In OSCC, JARID1B silencing is observed to attenuate sphere formation and stem cell marker expression (26). Additional findings have led to appreciation of the role of JARID1B in maintenance or differentiation of normal and malignant stem cell phenotypes (21, 27–29), suggesting broader utility as a CSC marker.

[1]Department of Otorhinolaryngology, University of Pennsylvania, Philadelphia, Pennsylvania. [2]Massachusetts General Hospital and Harvard Medical School, Boston, Massachusetts. [3]Department of Medicine, University of Pennsylvania, Philadelphia, Pennsylvania. [4]Department of Pathology, University of Pennsylvania, Philadelphia, Pennsylvania. [5]University Hospital, Essen, Germany. [6]Department of Biostatistics, University of Pennsylvania, Philadelphia, Pennsylvania. [7]The Wistar Institute, Philadelphia, Pennsylvania. [8]VA Medical Center, Philadelphia, Pennsylvania.

**Note:** Supplementary data for this article are available at Cancer Research Online (http://cancerres.aacrjournals.org/).

**Corresponding Author:** Devraj Basu, University of Pennsylvania, 3400 Spruce Street, 5 Ravdin/Silverstein, Philadelphia, PA 19104. Phone: 314-602-4129; Fax: 215-898-0980; E-mail: devraj.basu@uphs.upenn.edu

**doi:** 10.1158/0008-5472.CAN-15-3377

The unknown degree of identity between $G_0$-like and JARID1B$^{high}$ cells led us to evaluate their function, overlap, and developmental relationship. Here, we demonstrate that they are distinct subpopulations in OSCCs. Despite sharing stem cell–like function, only JARID1B$^{high}$ cells displayed conventional CSC-associated markers, PI3K pathway activation, and PI3K inhibitor sensitivity. However, $G_0$-like cells were primed to enter a JARID1B$^{high}$ state and required JARID1B to exert stem cell–like function. Our results have implications for maintenance of a dynamic CSC pool and provide insight into adaptation of oral CSCs to PI3K inhibition.

## Materials and Methods

### Cell lines, clinical specimens, vectors

Cells were maintained in 1:1 DMEM/F12 with 400 ng/mL hydrocortisone, 10% FBS, and 50 μg/mL gentimycin. SCC9 cells were obtained from ATCC. LNT14 cells are described (30). VU147T and CAL33 cells were gifts from Dr. Hans Joenje (VU Medical Center, Amsterdam, the Netherlands) and Dr. Jennifer Grandis (University of Pittsburgh, Pittsburgh, PA), respectively. Cell lines were authenticated using Identify Mapping Kit (Coriell). Clinical specimens were obtained under University of Pennsylvania Institutional Review Board protocol #417200 or Philadelphia VA protocol #01090. Lentiviral vectors pLU-JARID1Bprom-EGFP-Blast, pLU-CMVprom-EGFP-Blast, and pLKO-shJARID1B (20), transient expression vector pBIND-RBP2H1 (JARID1B; ref. 31), and retroviral vectors pWZ-neo-myrAKTΔ4-129-ER/A2myrAKTΔ4-129-ER (32, 33) are described.

### Flow cytometry and tumor cell purification

Antibodies are in Supplementary Table S1. Flow cytometry was performed using AstriosEQ (Beckman Coulter) or LSRII (BD Biosciences) instruments. Minced tumors were disrupted in 1 mg/mL collagenase IV using gentleMACS Dissociator (Miltenyi Biotec). Suspensions were agitated at 37°C for 1 hour before repeating disruption and 40-μm filtering. Mouse stromal cells were removed from xenografts by pretreating with anti-mouse CD16/32-Fc block and positive selection of human cells using anti-HLA-ABC. Mouse cell contamination was monitored using anti-mouse-H-2K$^d$. For human tissues, tumor cells were purified by negative selection with anti-CD45/CD31 as described previously (34). Dead cells were excluded by 7-aminoactinomycin D (7-AAD) throughout.

### Detection of $G_0$-like cells, ROS, label retention, ALDH activity

Tumor cells at $10^6$ cells/mL were incubated with 4 μmol/L Hoechst-33342 (Life Technologies) followed by 1 μg/mL Pyronin-Y (Sigma-Aldrich) at 37°C for 30 minutes. $G_0$-like cells were fluorescence-activated cell sorting (FACS)-purified by setting PyroninY$^{low}$ gates within the $G_0$–$G_1$ peak of the Hoechst-33342 profile. To detect ROS, cells were incubated with 2.5 μmol/L $H_2$DCFDA (Life Technologies) for 20 minutes at 37°C. PKH26/67 (Sigma-Aldrich) or CellTrace Violet (Life Technologies) were used as per manufacturer's instructions. Labeling (100%) was confirmed by flow cytometry; labeled cells were analyzed after 10 days of culture. Aldefluor assays were performed as per manufacturer's instructions (Stemcell).

### Western blotting

Protein lysates were made from equal cell numbers using Laemmli buffer, separated on 10% ECL gels (GE), and transferred to nitrocellulose using the Trans-Blot System (Bio-Rad). Antibodies (Supplementary Table S1) were incubated at 4°C overnight. After washing, blots were incubated with anti-Rabbit/Mouse IgG-DyLight and analyzed using a LI-COR Odyssey System (LI-COR).

### $G_0$-like cell detection in tissue

Paraffin-embedded samples were labeled using a multistep tyramide-amplified protocol as described previously (35). Following antigen retrieval and serum-free protein block, each labeling cycle consisted of primary antibody (Supplementary Table S1), secondary antibody conjugated to horseradish peroxidase, and TSA conjugated to a fluorophore (FITC/CY3/CY5, Perkin Elmer, Inc). Images were acquired on a Nikon Ti confocal microscope (60×). Tumor cells were distinguished with pan-cytokeratin staining. $G_0$-like cells were identified on the basis of the following pattern: DAPI + /AKT1$^{low}$/H3K9me2$^{low}$/HES1$^{high}$. Cells were counted in 10 random fields per section using ImageJ software. A blinded observer semiquantitatively assessed "high" or "low" fluorescence relative to background from isotype controls. Signals were designated "high" if the ratio of corrected total fluorescence was more than 2× compared with 3 "low" cells in the same image.

### Sphere formation

Ten cells per well were cultured in ultralow attachment 96-well plates (Corning) in serum-free complete MEGM (Lonza) for 14 days. Spheres were counted and imaged using a Leica DM IRB inverted microscope and iVision software (Biovision). Spheres were propagated by Accutase (Life Technologies) dissociation for 20 minutes and Trypan blue dead cell exclusion before replating.

### Mouse experiments

NOD/SCID/IL2 receptor γ-chain–deficient (NSG) mice were utilized under Wistar Institute IACUC protocols 112652/112655. Tumors were generated by subcutaneous flank injection of cells in 100 μL Matrigel (Corning). Tumors for drug studies were grown from $10^6$ cells to a volume of about 50 mm$^3$. GDC-0941 (SelleckChem) in 0.5% methylcellulose/0.2% Tween80 was administered at 100 mg/kg by daily oral gavage.

### Real-time reverse transcription PCR and RNA-Seq

RNA was isolated using the Qiagen RNeasy Kit (Qiagen). cDNA was generated from 1 μg RNA using RNA-to-DNA (Life Technologies) and PCR purification (Qiagen) kits. Expression was quantified using Power SYBR Green Master Mix and a Step-One Real-Time PCR System (Life Technologies). Primers are in Supplementary Table S2. RNA-Seq was performed on LNT14 cell fractions from 3 independent FACS isolations. Multiplexed Illumina libraries were prepared using Illumina stranded mRNA kits, pooled, and sequenced to 100 bp from one end of the insert. Aligning reads ($n = 236{,}908{,}957$) against the human genome (hg19) were detected using RUM v2.0.4. Uniquely aligning reads ($n = 215{,}252{,}518$) were used to quantify transcripts. Differential expression was defined using EdgeR with a generalized linear model to account for donor linkage and detect intertreatment differences. Multidimensional scaling plots confirmed significant donor effects. Differentially expressed genes had false discovery rate (FDR) > 10%. Gene Set Enrichment Analysis (GSEA) was performed using the MSigDB C2 v5.0 curated gene sets (>3,000)

to compare JARID1B$^{high}$, $G_0$-like, and bulk cells. A $\log_2$ fold change between paired conditions was used as a ranking variable.

### Statistics and tumor-initiating cell frequency

Data are expressed as mean ± SE. At least three independent replicates were performed per experiment. ANOVA or *t* tests evaluated differences among means. Tukey procedure tested pairwise differences for significant ANOVAs. An *F* statistic tested for equal variances. For unequal variances, Welch ANOVA or *t* statistics were used. Mann–Whitney *U* tests were used for variables lacking normal distribution. Differences between cumulative distributions for latency times were defined using Kaplan–Meier and exact log-rank tests. Tumor-initiating cell (TIC) frequencies were estimated using ELDA software (http://bioinf.wehi.edu.au/software/elda/; ref. 36).

## Results

### $G_0$-like OSCC cells exhibit stem cell–like function

$G_0$-like cells were identified by flow cytometry within multiple OSCC cell lines using Hoechst-33342 and Pyronin-Y to detect RNA$^{low}$ cells within the $G_0$–$G_1$ cell-cycle peak (Fig. 1A, left and Supplementary Fig. S1A). $H_2$DCFDA staining confirmed the fraction to be ROS$^{low}$ (Fig. 1A, right and Supplementary Fig. S1B, left), consistent with the $H_2$DCFDA-based definition of $G_0$ -like breast cancer cells (11). $G_0$-like cells in cell lines showed high p27$^{Kip1}$ and Hes1, along with decreased total Akt protein (Fig. 1B and Supplementary Fig. S1B, right). Continued cyclin D1 expression implied a lack of complete $G_0$ cell-cycle exit, supporting the "$G_0$-like" designation. Applying the Pyronin-Y–based isolation strategy to tumor cells purified from clinical specimens and patient-derived xenografts (PDX) also detected $G_0$-like cells with low ROS and Akt (Supplementary Fig. S1C and S1D). Similar cells were stained by established methodology in sections of 9 human tumors and 2 derivative PDXs. Cells with the Hes1$^{high}$/Akt$^{low}$/H3K9me2$^{low}$ staining profile of ROS$^{low}$ $G_0$-like breast cancer cells (11) were detectable as a minority fraction in most samples (Fig. 1C). $G_0$-like fractions from cell lines were tested in clonal sphere assays, where they showed enhanced formation of primary spheres and propagation as secondary spheres (Fig. 1D). They also formed tumors at higher incidence and shorter latency than the non–$G_0$-like fraction upon xenotransplantation at low cell dose (Fig. 1E). $G_0$-like cells isolated from PDXs also had enhanced tumor-initiating capacity, forming tumors with similar efficiency to CD44$^{high}$ cells (Fig. 1F, top) despite being CD44$^{low}$ (bottom and Supplementary Fig. S1E). Together, these results established that $G_0$-like OSCC cells can display CSC function. Clinicopathologic traits for patient tumors, along with their derivative PDXs and cell lines, are in Supplementary Table S3.

### JARID1B is a distinct basis for detecting CSC function

The quiescent and stem cell–like traits of $G_0$-like cells appeared comparable with those of melanoma cells expressing high JARID1B (20). To assess the role of JARID1B in the oral CSC pool, a promoter-based reporter for JARID1B transcription, J1BpromEGFP (20), was stably expressed in OSCC cell lines. LNT14 and SCC9 cells with 5% highest EGFP expressed increased JARID1B mRNA and protein (Fig. 2A and Supplementary Fig. S2A) and were designated JARID1B$^{high}$. All subsequent studies were standardized to assess changes in JARID1B$^{high}$ population size relative to this 5% EGFP$^{high}$ reference gate in control cells. The label retention and CSC function previously seen in a JARID1B$^{high}$ state defined identically for melanoma (20) were evaluated in OSCC. Fluorescent membrane labeling showed that in contrast to the $G_0$-like fraction, JARID1B$^{high}$ OSCC cells were highly label-retaining over 10 days, indicating low turnover (Supplementary Fig. S2B). However, JARID1B$^{high}$ cells were distributed outside the $G_0$-like gate instead showing $G_2$–M expansion (Fig. 2B and Supplementary Fig. S2C and S2D), suggesting slowed $G_2$–M transit over $G_0$-like arrest. Decreased JARID1B reporter function and protein in the $G_0$-like gate (Supplementary Fig. S2E) distinguished the 2 states beyond cell-cycle status, raising the possibility that JARID1B$^{high}$ and $G_0$-like cells are distinct subpopulations. Thus, subsequent studies standardized comparison of mutually exclusive $G_0$-like and JARID1B$^{high}$ gates to a "bulk" gate that excludes both subsets (Supplementary Fig. S3A).

In functional analyses, JARID1B$^{high}$ cells defined by the 5% reference gate in monolayer culture increased in clonal spheres (Fig. 2C and Supplementary Fig. S3B) and showed higher primary and secondary sphere-forming capacity (Fig. 2D). JARID1B$^{high}$ cells from 2 lines formed xenografts with comparable efficiency to $G_0$-like cells but higher incidence and shorter latency than bulk cells, with all fractions producing tumors with indistinguishable histology (Fig. 2E and Supplementary Fig. S3C and S3D). Limiting dilution showed JARID1B$^{high}$ LNT14 cells to form 100% tumors even at a dose of 10 cells and the $G_0$-like subset to have markedly higher TIC frequency than bulk cells (Supplementary Fig. S3E). Reliance on a reporter to purify JARID1B$^{high}$ cells prevented their direct isolation from PDXs for functional testing. However, their overlap with the CD44$^{high}$ fraction by was supported by flow cytometric analysis of cell lines and PDX tumors (Fig. 2F and G, left and Supplementary Fig. S3F, top) and detection of elevated JARID1B expression in CD44$^{high}$ PDX cells (Fig. 2G, right and Supplementary Fig. S3F, bottom). Together, these data suggested that JARID1B$^{high}$ and $G_0$-like cells are subpopulations with distinct molecular characteristics but similar stem cell–like function.

### JARID1B$^{high}$ and $G_0$-like cells show divergent molecular profiles and PI3K signaling

Shared stem cell–like function between $G_0$-like and JARID1B$^{high}$ cells despite divergent CD44 expression justified further molecular comparisons. Only JARID1B$^{high}$ cells increased expression of the pluripotency-related factors Oct4 and Bmi1 (Fig. 3A) and another oral CSC marker *ALDH1A1* (Fig. 3B, left), the isoform underlying increased ALDH activity in OSCC (37). High ALDH activity in Aldefluor assays also corresponded with high levels of JARID1B (Fig. 3B, right). Broader comparison of $G_0$-like, JARID1B$^{high}$, and bulk cells was performed by mRNA sequencing. Pairwise comparison of $G_0$-like versus JARID1B$^{high}$ subsets to bulk cells revealed 61 genes upregulated by both subsets (Fig. 3C and Supplementary Tables S4–S7), including most transcripts increased in $G_0$-like cells. This significant overlap suggested a close relationship between the 2 states; however, minimal overlap existed between genes downregulated by $G_0$-like versus JARID1B$^{high}$ cells (Supplementary Fig. S4A). Hierarchical clustering of gene-scaled expression levels confirmed that $G_0$-like and JARID1B$^{high}$ cells clustered more closely to each other than to bulk cells (Supplementary Fig. S4B). Among the gene sets, most significantly upregulated in $G_0$-like and JARID1B$^{high}$ cells (Supplementary Tables S8–S10) were signatures defined in mammary and stromal stem cells (Fig. 3D, left and Supplementary Fig. S4C, left; refs. 38, 39), consistent with their shared CSC function.

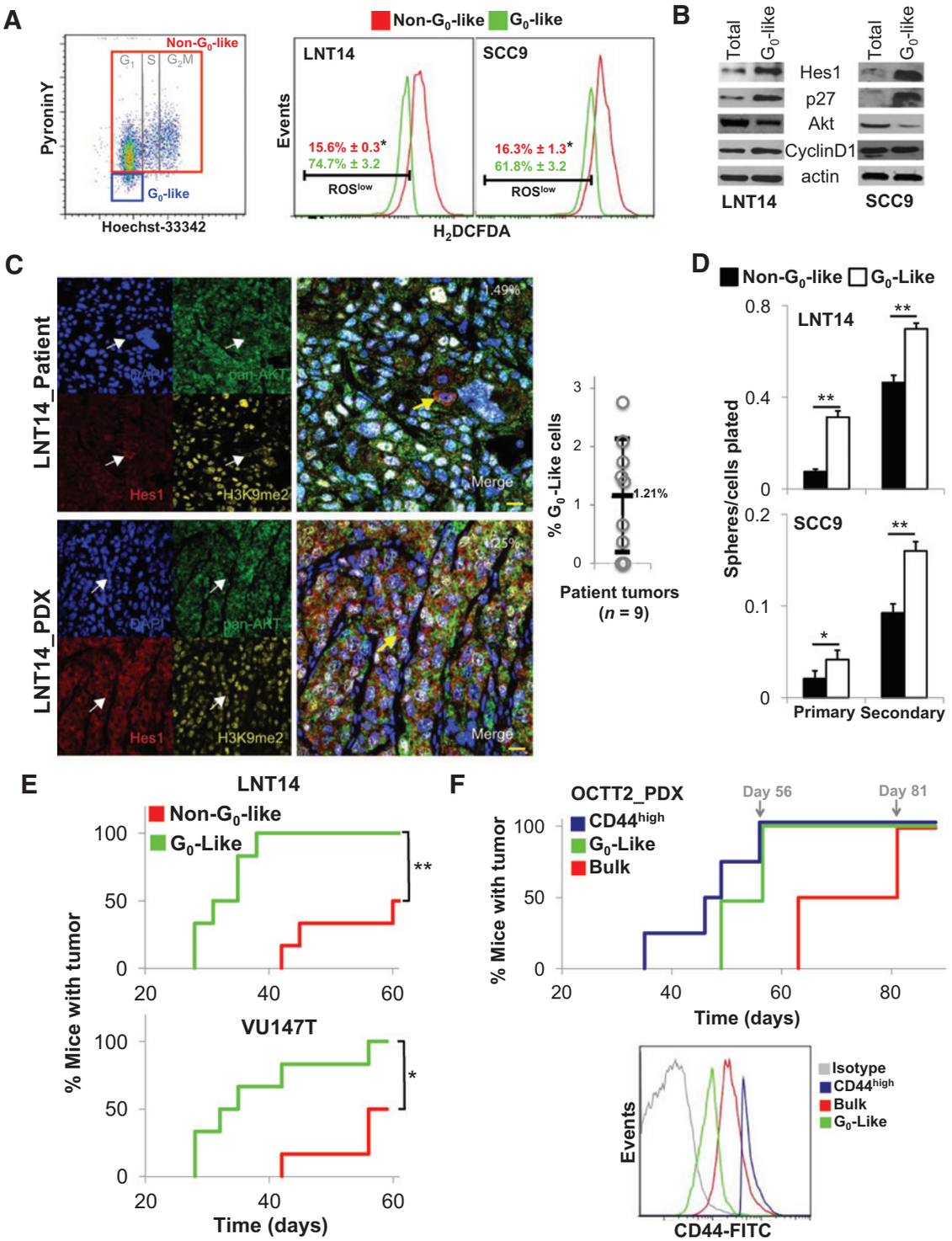


**Figure 1.**

$G_0$-like cells exhibit stem cell-like function. **A,** flow cytometry plot illustrates $G_0$-like gate in representative LNT14 cell line (left). $H_2$DCFDA profiles compare $G_0$-like with non–$G_0$-like fractions in OSCC lines (right). *, $P < 0.001$; **, $P < 0.0001$. **B,** Western blot analyses of $G_0$-like and unfractionated (total) cells from OSCC lines. **C,** confocal immunofluorescence of patient tumor and derivative PDX stained for H3K9me2 (yellow), Hes1 (red), pan-Akt (green), and DAPI (blue). Arrows, $G_0$-like cells (H3K9me2$^{low}$/HES1$^{high}$/pan-AKT$^{low}$; left). Bar, 10 μm. Staining quantifies $G_0$-like cells in 9 patient tumors (right). **D,** primary and secondary sphere formation by $G_0$-like versus non–$G_0$-like fractions of OSCC lines. *, $P < 0.05$; **, $P < 0.0001$. **E,** xenograft growth of $G_0$-like versus non–$G_0$-like fractions from cell lines LNT14 (100 cells/mouse, $n = 6$/group) and VU147T (1,000 cells/mouse, $n = 6$/group). *, $P < 0.025$; **, $P < 0.0025$. **F,** xenograft growth (top) and cell surface CD44 (bottom) from $G_0$-like, CD44$^{high}$, and bulk fractions of OCTT2 PDX (2,000 cells/mouse, $n = 4$/group). Latency for $G_0$-like and CD44$^{high}$ cells were shorter than for bulk cells ($P < 0.025$).

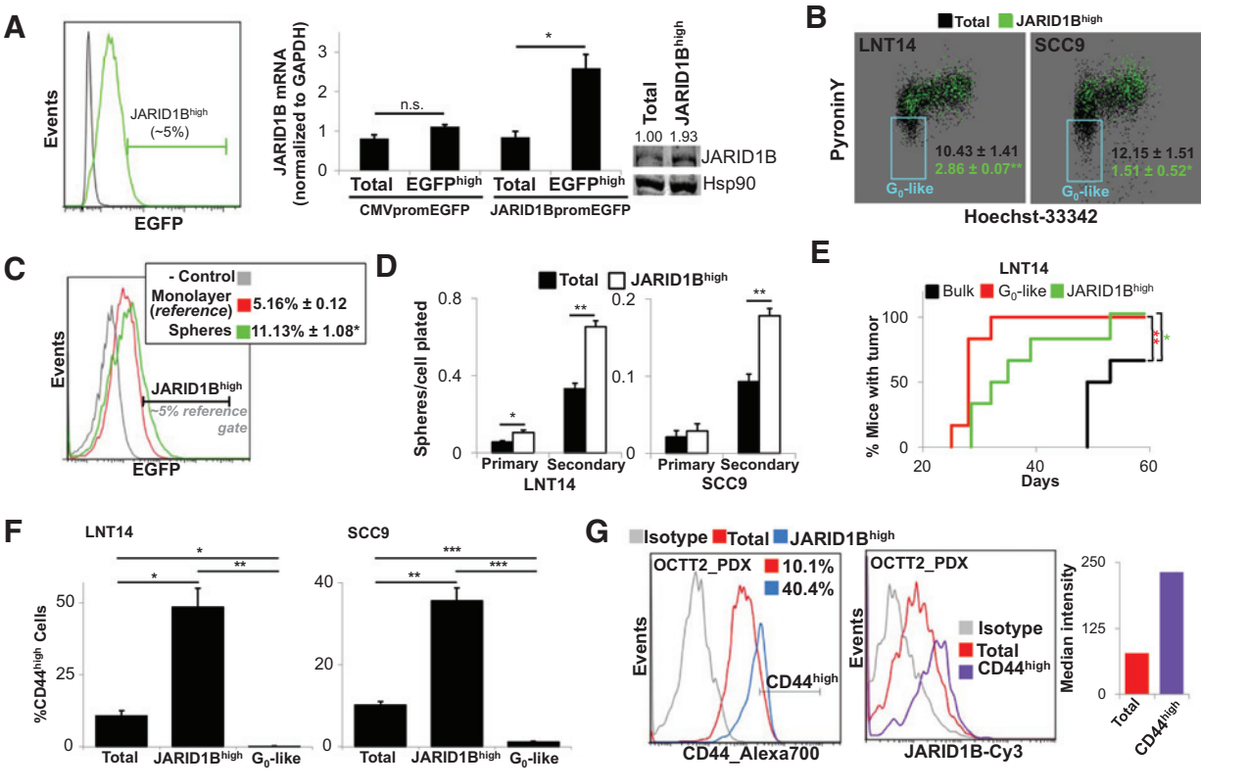


**Figure 2.**

JARID1B is a distinct basis for detecting CSC function. **A,** standardized 5% JARID1B$^{high}$ reference gate illustrated in LNT14_J1BpromEGFP cells (left). JARID1B expression in the EGFP$^{high}$ fraction of LNT14_J1BpromEGFP or control LNT14_CMVpromEGFP cells by qRT-PCR (middle; *, $P < 0.025$). JARID1B protein in JARID1B$^{high}$ cells by Western blotting (left; values indicate JARID1B normalized to loading control). **B,** Pyronin-Y/Hoechst-33342 plots distinguish cell-cycle profiles of $G_0$-like and JARID1B$^{high}$ fractions. *, $P < 0.0005$. **C,** profiles show JARID1B$^{high}$ fraction size in spheres of LNT14_J1BpromEGFP cells based on the 5% reference gate set in monolayer culture. *, $P < 0.01$. **D,** primary and secondary sphere formation by JARID1B$^{high}$ versus total cells. *, $P < 0.0005$; **, $P < 0.0001$. **E,** xenograft formation by $G_0$-like, JARID1B$^{high}$, or bulk LNT14_J1BpromEGFP cells (100 cells/mouse, $n = 6$/group). *, $P < 0.05$; **, $P < 0.0025$. **F,** localization of JARID1B$^{high}$ cells to the top 10% CD44$^{high}$ fraction in cell lines (left) was quantified (right). *, $P < 0.05$; **, $P < 0.005$. **G,** localization of JARID1B$^{high}$ PDX cells to the top 10% CD44$^{high}$ fraction (left) and JARID1B expression by flow cytometry in this CD44$^{high}$ fraction (right), determined by intracellular JARID1B immunofluorescence after surface CD44 staining.

Notably, these GSEA profiles were more prominent in JARID1B$^{high}$ over $G_0$-like cells (Fig. 3D, right and Supplementary Fig. S4C, right). JARID1B$^{high}$ cells also more strongly upregulated an epithelial-to-mesenchymal transition profile from breast CSCs (Fig. 3E, left; ref. 40). These findings reveal distinctions between $G_0$-like and JARID1B$^{high}$ cells despite shared expression of a core gene set, with JARID1B$^{high}$ cells consistently exhibiting a more conventional CSC-related profile.

Further analyses dissected the proliferative states of the subsets. Despite JARID1B$^{high}$ cells retaining label, only $G_0$-like cells downregulated cell-cycle–related gene transcription on the basis of a Reactome database gene set (Fig. 3E, right and Supplementary Fig. S4D). To further characterize this difference, proliferative oncogenic signals were compared across cell fractions. No differences were evident in MAPK or JAK/STAT signaling based on ERK and STAT3 phosphorylation, respectively (Supplementary Fig. S4E). The reduced PI3K activity anticipated in $G_0$-like cells based on low total Akt was confirmed at the level of phospho-Akt (Supplementary Figs. S2E and S4F). However, high phosphorylation of Akt and downstream target GSK3β indicated pathway hyperactivation in JARID1B$^{high}$ cells relative to bulk (Fig. 3F and Supplementary Fig. S2E), adding to parallels between JARID1B$^{high}$ cells and other CSC phenotypes (15–18). In contrast, AKT suppression in $G_0$-like cells suggested a distinct role in the CSC pool.

### $G_0$-like cells are primed to become JARID1B$^{high}$

The functional properties shared by $G_0$-like and JARID1B$^{high}$ cells prompted assessment of whether $G_0$-like CSC function arises from transition to a JARID1B$^{high}$ state. The capacity of $G_0$-like versus bulk cells to upregulate JARID1B was tested by FACS purification and reculturing. $G_0$-like cells reconstituted the original JARID1B$^{high}$ fraction by day 4, whereas bulk cells failed to do so fully over 14 days (Fig. 4A and Supplementary Fig. S5A). However, despite their higher capacity to become JARID1B$^{high}$, purified $G_0$-like cells proliferated comparably to bulk cells (Supplementary Fig. S5B). Thus, we tested whether $G_0$-like cells must return to rapid proliferation before becoming JARID1B$^{high}$ or can transition directly. Comparison of cultures grown from purified $G_0$-like versus bulk cells labeled with CellTrace revealed 2-fold more cells retaining label among JARID1B$^{high}$ cells arising from the $G_0$-like subset (Fig. 4B). A proximate relationship between the $G_0$-like and JARID1B$^{high}$ states was further supported by efficient $G_0$-like to JARID1B$^{high}$ transition observed during sphere

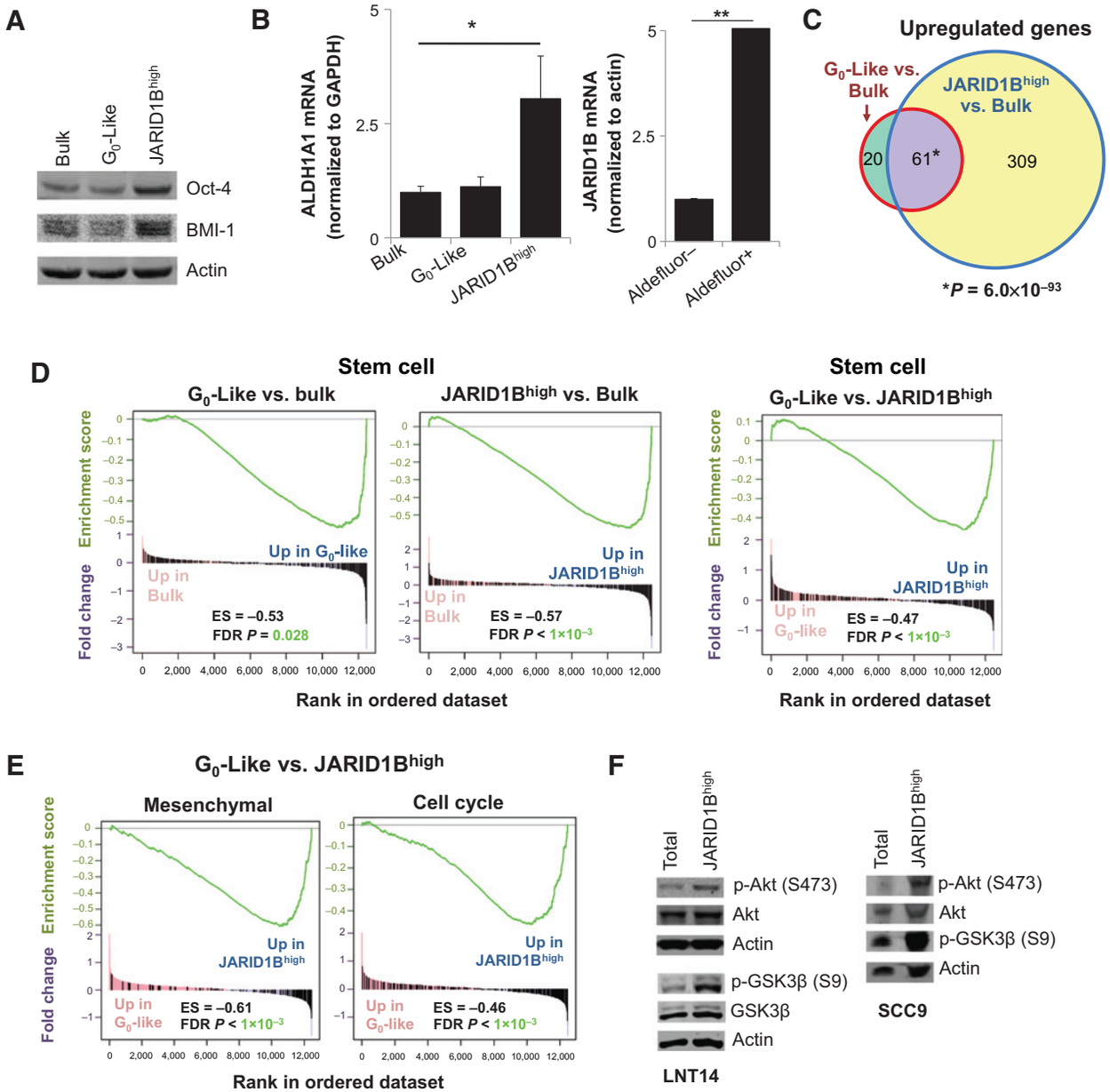


**Figure 3.**

JARID1B$^{high}$ and $G_0$-like cells exhibit divergent molecular profiles and PI3K signaling. **A,** Western blot analyses for indicated markers in $G_0$-like, JARID1B$^{high}$, and bulk LNT14 cells. **B,** qRT-PCR for ALDH1A1 in $G_0$-like, JARID1B$^{high}$, and bulk LNT14 cells (left) and JARID1B in Aldefluor$^{+}$ versus Aldefluor$^{-}$ cells. *, $P < 0.05$; **, $P < 0.001$. **C,** genes upregulated relative to bulk in $G_0$-like and JARID1B$^{high}$ LNT14 cells. **D,** GSEAs show the Lim_Mammary_Stem_Cell_Up gene set for the indicated pairwise comparisons. ES, enrichment score; FDR, false discovery rate. **E,** GSEAs for Sarrio_Epithelial_Mesenchymal_Transition_Up (left) and Reactome_Cell_Cycle (right) gene sets in $G_0$-like versus JARID1B$^{high}$ LNT14 cells. **F,** Western blot analyses WBs of JARID1B$^{high}$ versus total cells.

formation, where $G_0$-like cells generated spheres containing more JARID1B$^{high}$ cells than bulk spheres (Fig. 4C). Here JARID1B upregulation by $G_0$-like cells was reflected by appearance of a second EGFP peak in a bimodal distribution, which was absent or less prominent in bulk-derived spheres (Fig. 4D). Together, these data support a developmental relationship in which $G_0$-like cells are primed to become JARID1B$^{high}$.

### $G_0$-like cells exert CSC function by a JARID1B-dependent mechanism

The priming of $G_0$-like cells to become JARID1B$^{high}$ led to testing whether JARID1B directly contributes to the transition. When JARID1B was reduced using an shRNA of established specificity (Fig. 5A and Supplementary Fig. S5C; ref. 20), LNT14 cells in the $G_0$-like gate after JARID1B knockdown

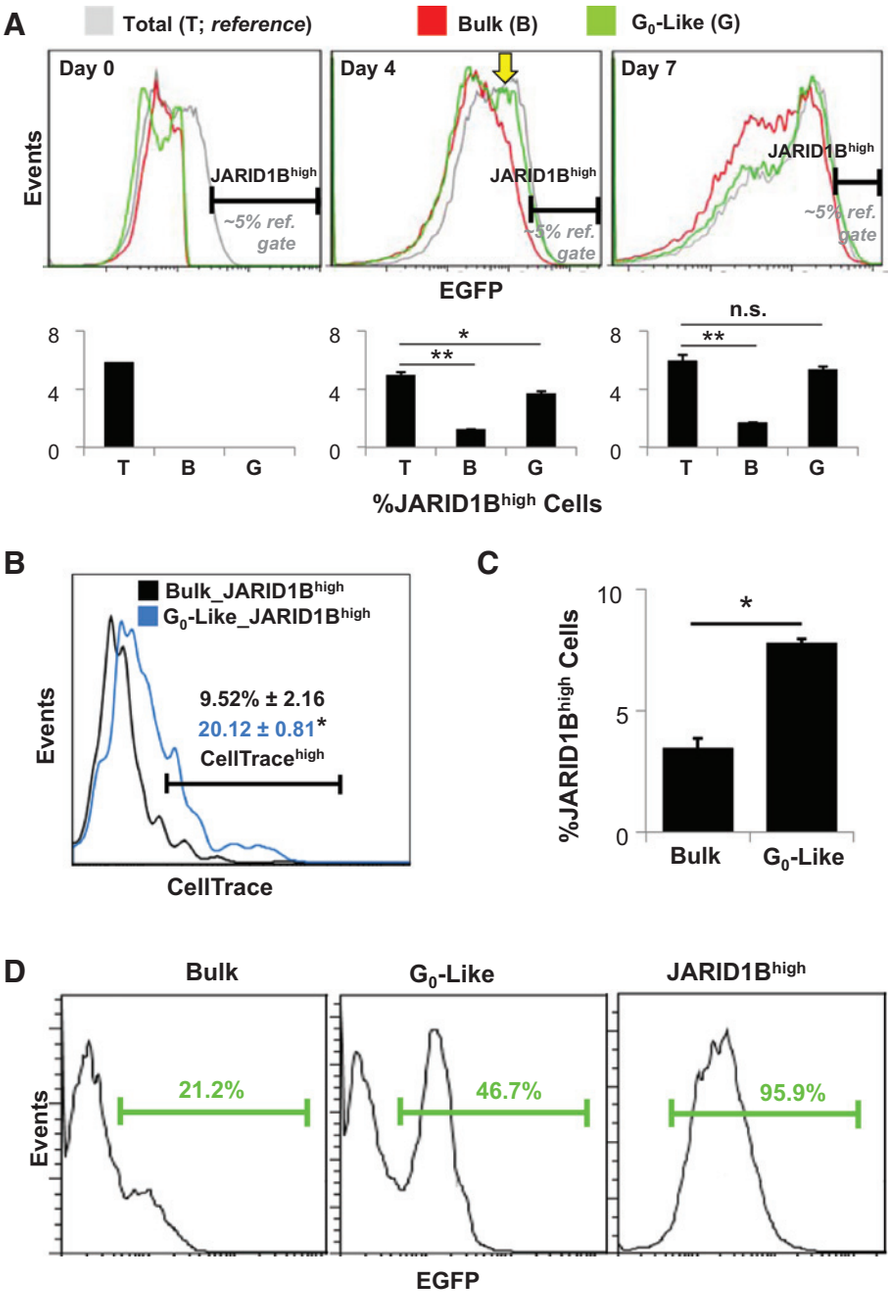


**Figure 4.**

$G_0$-like cells are primed to become JARID1B$^{high}$. **A,** histograms illustrate JARID1B$^{high}$ gate in purified $G_0$-like, bulk, and total LNT14_J1BpromEGFP cells on culture day 0, 4, and 7. Arrow, $G_0$-like cells shifting to the JARID1B$^{high}$ fraction. Quantification below. *, $P < 0.0025$; **, $P < 0.0001$. n.s., not significant. **B,** CellTrace label retention by JARID1B$^{high}$ fraction arising from $G_0$-like versus bulk cells after 10-day culture. *, $P < 0.0025$. **C**, JARID1B$^{high}$ cell content in spheres generated from $G_0$-like versus bulk LNT14_J1BpromEGFP cells. *, $P < 0.0001$. **D**, EGFP fluorescence within spheres from $G_0$-like, JARID1B$^{high}$, and bulk LNT14_J1BpromEGFP cells. Gates define the more intense fluorescence peak.

retained low ROS and Akt (Supplementary Fig. S5D). However, their sphere-forming capacity decreased to that of bulk cells, whose function was unaltered by shRNA (Fig. 5B and Supplementary Fig. S5E) and tumorigenesis by $G_0$-like cells diminished to the incidence and latency of bulk cells (Fig. 5C). These results could arise from reduced JARID1B preventing acquisition of oral CSC markers or from impairment of subsequent CSC function. The former was supported by accumulation of $G_0$-like cells upon JARID1B silencing (Fig. 5D and Supplementary Fig. S5F). Under silencing conditions, the 5% EGFP$^{high}$ cells, which are expected to maintain high JARID1B transcription, were similar in frequency to control EGFP$^{high}$ (i.e., JARID1B$^{high}$) cells but lacked high JARID1B mRNA (Supplementary Fig. S5G). Such JARID1B-silenced EGFP$^{high}$ cells showed decreased sphere formation (Fig. 5E, left and Supplementary Fig. S5E) and lower Oct4 and Bmi1 (Fig. 5E, right), supporting the direct role of JARID1B in acquisition of CSC markers and function. This finding agreed with marker and functional shifts observed during JARID1B knockdown or overexpression. Specifically, knockdown decreased surface CD44, *ALDH1A1* mRNA, and ALDH activity (Fig. 5F and Supplementary Fig. S5H), whereas overexpression increased CD44 and *ALDH1A1* coordinately with sphere formation (Fig. 5G). In sum, these results indicate

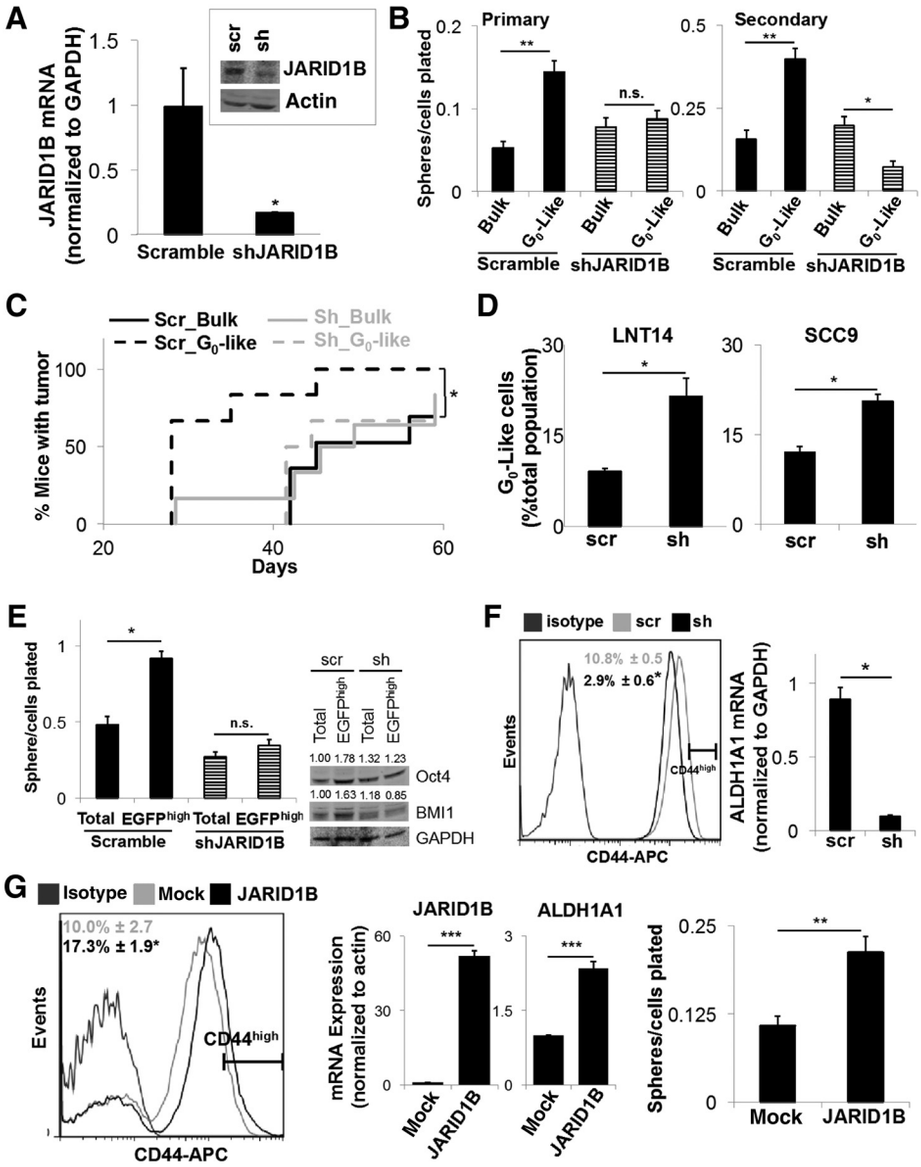


**Figure 5.**
$G_0$-like cells exert CSC function by a JARID1B-dependent mechanism. **A,** JARID1B by qRT-PCR and Western blotting (inset) in LNT14 cells expressing scramble (scr) or JARID1B (sh) shRNA. *, $P < 5 \times 10^{-5}$. **B,** primary and secondary spheres from $G_0$-like and bulk LNT14 cells expressing sh versus scr. *, $P < 0.0005$; **, 0.0001. **C,** xenograft formation by $G_0$-like or bulk fractions from sh versus scr LNT14 cells (100 cells/mouse, $n = 6$/group). *, $P < 0.025$. **D,** $G_0$-like fraction size in 2 sh versus scr cell lines. *, $P < 0.025$. **E,** sphere formation (left) and Oct4/BMI1 WB (right) for $EGFP^{high}$ and total fractions in sh or scr LNT14_J1BpromEGFP cells. Band densities are normalized to GAPDH. *, $P < 0.0001$. **F,** CD44 by flow cytometry and ALDH1A1 by QRT-PCR in sh versus scr LNT14 cells. *, $P < 0.0001$. **G,** CD44 and ALDH1A1 in LNT14 cells after JARID1B cDNA or mock transfection (left). Sphere formation by transfected cells (right). *, $P < 0.05$; **, $P < 0.025$; ***, $P < 0.0005$. n.s., nonsignificant.

that JARID1B contributes to the function of $G_0$-like cells by driving them toward the $JARID1B^{high}$ molecular profile.

### PI3K signals regulate the $G_0$-like to $JARID1B^{high}$ transition

Although JARID1B silencing blocked CSC marker acquisition, global pAkt levels were unaltered (Fig. 6A, left) and Akt hyperactivation in $EGFP^{high}$ cells was maintained (right). This result suggested that PI3K signals act proximal to JARID1B to drive the transition. To test this possibility, Akt was activated in LNT14_J1BpromEGFP cells carrying a myristoylated Akt variant fused to an estrogen receptor domain (myrAktER) that blocks activation in absence of 4-hydroxytamoxifen (4-OHT; Supplementary Fig. S6A; ref. 32). Addition of 4-OHT expanded $JARID1B^{high}$ cells (Fig. 6B), supporting PI3K signaling driving entry into this state. Likewise, PI3K inhibition *in vitro* with LY294002 at about 25% growth-inhibitory dose with minimal cytotoxicity (Supplementary Fig. S6B) decreased both the $JARID1B^{high}$ fraction (Fig. 6C, left and Supplementary Fig. S6C, left) and JARID1B protein (Fig. 6C, right). In contrast, the $G_0$-like fraction markedly expanded upon treatment with LY294002 or the clinical pan-PI3K inhibitor GDC-0941 (Fig. 6D and Supplementary Fig. S6C, right) at doses producing modest growth inhibition (Supplementary Fig. S6B). $G_0$-like cells isolated after GDC-0941 treatment retained sphere-forming capacity (Fig. 6E, left) and tumorigenicity (right), providing evidence of their PI3K inhibitor resistance. Xenografts established from LNT14_J1BpromEGFP cells were also treated *in vivo* with GDC-0941 at growth-inhibitory doses (Fig. 6F, left). Analysis of disaggregated residual tumors revealed no $JARID1B^{high}$ cell enrichment and a trend toward their decreased percentage (Fig. 6F, middle). Concurrently, there was greater than 2-fold expansion of $G_0$-like cells (right). Expanded $G_0$-like subsets in treated tumors were verified by quantification of $Hes1^{high}/Akt^{low}/H3K9me2^{low}$ cells in tumor sections (Fig. 6G). In sum, our findings support a model in which

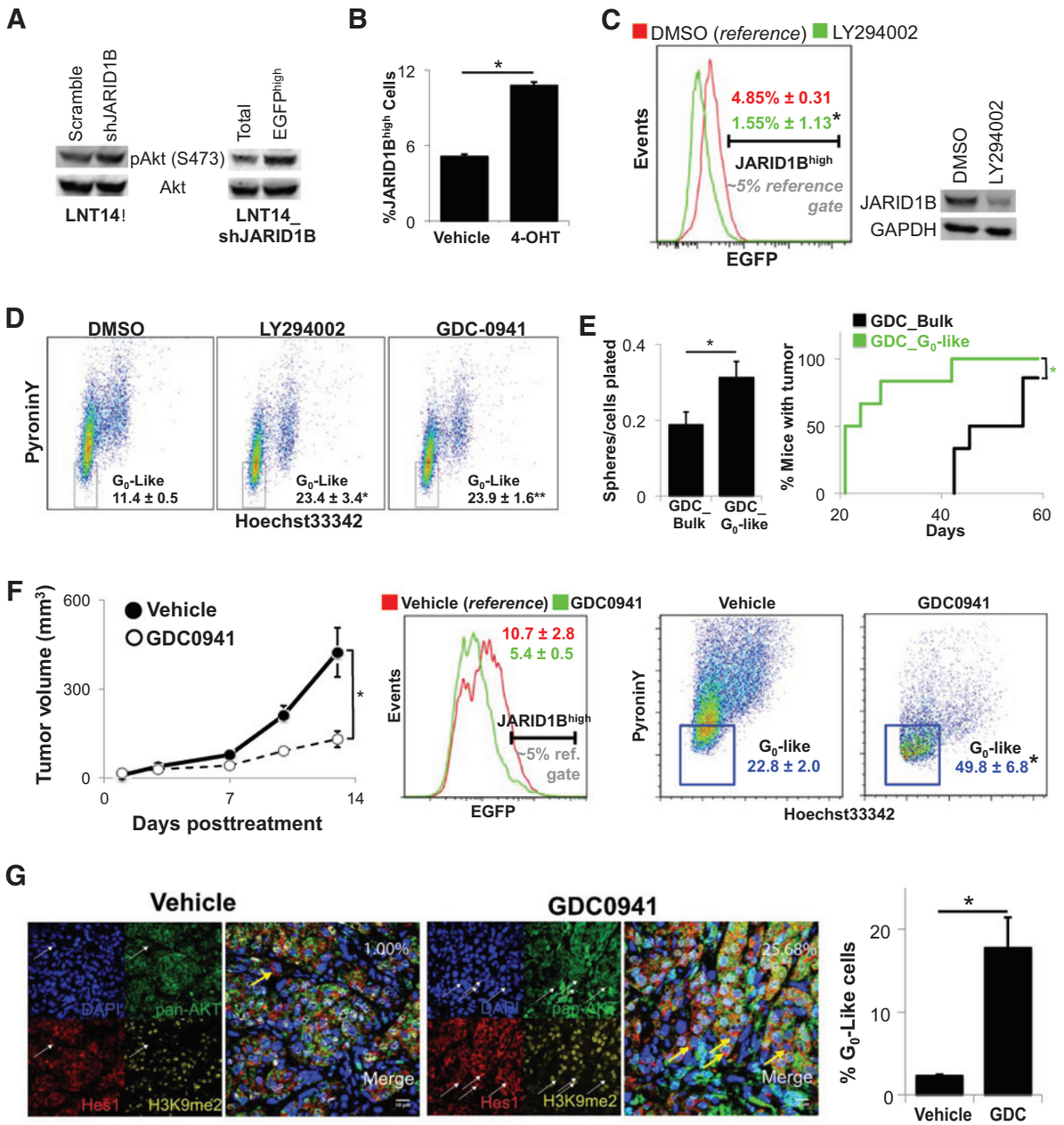


**Figure 6.**

PI3K signals regulate the $G_0$-like to JARID1B$^{high}$ transition. **A,** Akt and pAkt by Western blotting in sh versus scr LNT14 cells (left) and EGFP$^{high}$ versus total LNT14_J1BpromEGFP_shJARID1B cells (right). **B,** JARID1B$^{high}$ fraction size in LNT14_J1BpromEGFP_myrAktER cells treated with 10 nmol/L 4-hydroxytamoxifen (4-OHT) for 72 hours. *, $P < 0.0001$. **C,** LNT14_J1BpromEGFP cells treated with 10 μmol/L LY294002 for 72 hours were analyzed for EGFP (left) and JARID1B by Western blotting (right). *, $P < 0.01$. **D,** $G_0$-like cell content after LY294002 or 250 nmol/L GDC-0941 treatment. *, $P < 0.01$; **, $P < 0.0001$ **E,** $G_0$-like and bulk LNT14_J1BpromEGFP cells purified after 72 hours of GDC-0941 (GDC) treatment were analyzed for sphere (left) and xenograft (right; 100 cells/mouse, $n = 6$/group) formation. *, $P < 0.05$. **F,** LNT14_J1BpromEGFP xenograft growth during GDC treatment (left; $n = 5$/group). Tumors were analyzed for JARID1B$^{high}$ cells (middle) and $G_0$-like cells (right). *, $P < 0.025$. **G,** confocal immunofluorescence of tumor sections from GDC- or vehicle-treated mice were stained as in Fig. 1E. Arrows indicate $G_0$-like cells (H3K9me2$^{low}$/HES1$^{high}$/pan-AKT$^{low}$; left), which were quantified for GDC versus vehicle groups (right, $n = 4$ tumors/group). *, $P < 0.05$.

PI3K-dependent JARID1B upregulation drives the $G_0$-like to JARID1B$^{high}$ state transition (Fig. 7). Therapeutic PI3K inhibition is therefore predicted to expand the $G_0$-like compartment while depleting JARID1B$^{high}$ cells.

## Discussion

A potential barrier to CSC-directed therapy arises from evidence that some cells lacking CSC markers retain stem cell-like

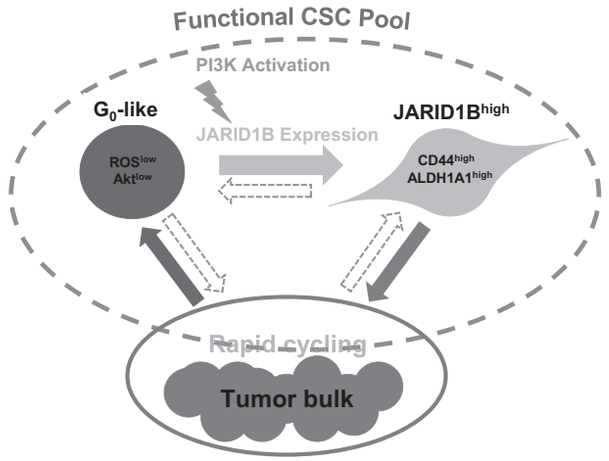


**Figure 7.**
Model of $G_0$-like and JARID1B$^{high}$ cells as related subsets of the oral CSC pool. $G_0$-like cells exert stem cell–like function by PI3K-mediated entry to a JARID1B$^{high}$ state. They are shown arising from rapid-cycling cells based on prior work (11). Dotted arrows represent transitions potentially impacting CSC homeostasis that are not addressed here.

functional capacity (20, 41, 42). Here we show that a $G_0$-like subset lacking standard oral CSC markers is primed for stem cell–like function through transition into a state expressing such markers. The transition was mediated by PI3K-dependent upregulation of the histone demethylase JARID1B. Regulation of a heterogeneous CSC pool by this mechanism may provide a novel basis for its homeostasis during therapy.

By establishing the function of JARID1B in mediating the CSC potential of $G_0$-like cells, our results expand understanding of its context-specific roles in malignant and normal stem cell homeostasis. JARID1B promotes either maintenance or differentiation of various normal stem cell populations (29, 43) at least partly through silencing lineage specification gene promoters (21, 44). In malignancy, increased JARID1B expression or amplification occur in multiple tumor types (23–25). Its oncogenic function is best characterized in breast cancer, where overexpression drives a luminal cell–specific expression program (23). In contrast, JARID1B is not overexpressed in melanomas but still underlies the function of a subset of JARID1B$^{high}$ cells with a role in tumor maintenance and drug resistance (19, 20). Because JARID1B protein is widely detectable in OSCCs (26), CSC function associated with the rare JARID1B$^{high}$ cells studied here may occur through dose-dependent effects on a subset of JARID1B-regulated genes. This gene regulation is also likely impacted by the known interactions of JARID1B with other transcriptional and epigenetic regulators that vary based on cellular context (25, 45–47).

Including $G_0$-like cells in the CSC pool in our model (Fig. 7) emphasizes their potential for stem cell–like function. $G_0$-like cells have been shown to arise from asymmetric division of rapidly cycling cells as a stochastic event (11, 13). This event was mediated by a novel integrin-regulated signaling cascade leading to proteasomal Akt1 degradation via E3 ubiquitin ligase TTC3 (13) and may allow them to serve as an intermediate for transition to the JARID1B$^{high}$ state. Although PI3K activation was observed here to drive this transition, it is unclear what signals initiate it or whether additional pathways permit $G_0$-like cells to return to rapid proliferation without a JARID1B$^{high}$ intermediate. Detailing such mechanisms may offer approaches to addressing $G_0$-like cells as a potential basis for innate therapy resistance.

The dichotomous PI3K activation in $G_0$-like versus JARID1B$^{high}$ cells offers insight into the role of the pathway in homeostasis of the oral CSC pool and its adaptation to PI3K inhibition. Putative CSCs in multiple tumor types exhibit PI3K hyperactivation and small-molecule inhibitor sensitivity (15–18). Our similar finding in JARID1B$^{high}$ OSCC cells is particularly relevant given the frequent driving PI3K pathway alterations in OSCC (48), which include isolated PIK3CA mutations for some HPV-positive tumors (49). Our results suggest that $G_0$-like cells may be a reservoir that replenishes the JARID1B$^{high}$ CSC state upon depletion by PI3K inhibition. Such effects may explain why PI3K pathway inhibitors generally produce modest clinical responses, despite the predicted sensitivity of the CSC pool. In this context, $G_0$-like cells may play a role in therapy resistance parallel to that of reserve stem cells recruited during injury responses in normal epithelia. For example, loss of proliferative Lgr5-positive intestinal stem cells through injury leads to their regeneration by quiescent Bmi1-positive cells that have limited roles in normal homeostasis (50). Similar plasticity among quiescent and proliferative adult stem cells is seen in multiple tissue types (7, 8) and likely is maintained and exploited by solid tumors.

Although absence of rapid proliferation in $G_0$-like and JARID1B$^{high}$ cells may confer drug resistance to both subsets, their divergent PI3K activation and cell-cycle states suggest a need for differing targeting strategies. One approach may be to block entry into the $G_0$-like state in combination with PI3K inhibition. In addition to addressing mechanisms regulating the $G_0$-like pool, further work is needed to test how molecular alterations in the PI3K pathway impact the size of $G_0$-like versus JARID1B$^{high}$ subsets and their dynamics in response to PI3K inhibition. Likewise, studies are needed to test how the oral CSC pool is regulated by individual downstream components of the PI3K pathway. Together, such work may facilitate combination therapies to deplete all cell phenotypes cooperatively sustaining the oral CSC pool.

## Disclosure of Potential Conflicts of Interest

G.S Weinstein has provided expert testimony for Olympus Inc. S. Ramaswamy is a consultant/advisory board member of Tesaro. No potential conflicts of interest were disclosed by the other authors.

## Authors' Contributions

**Conception and design:** N.D. Facompre, S. Kabraji, M. Herlyn, A.K. Rustgi, D. Basu

**Development of methodology:** N.D. Facompre, S. Kabraji, V. Sahu, A. Roesch, D. Basu

**Acquisition of data (provided animals, acquired and managed patients, provided facilities, etc.):** N.D. Facompre, K.M. Harmeyer, S. Kabraji, Z. Belden, V. Sahu, K. Whelan, D. Basu

**Analysis and interpretation of data (e.g., statistical analysis, biostatistics, computational analysis):** N.D. Facompre, X. Sole, S. Kabraji, A. Roesch, P.A. Gimotty, H. Nakagawa, S. Ramaswamy, D. Basu

**Writing, review, and/or revision of the manuscript:** N.D. Facompre, K.M. Harmeyer, X. Sole, S. Kabraji, V. Sahu, G.S. Weinstein, A. Roesch, P.A. Gimotty, A.K. Rustgi, H. Nakagawa, S. Ramaswamy, D. Basu

**Administrative, technical, or material support (i.e., reporting or organizing data, constructing databases):** G.S. Weinstein, A. Roesch, S. Ramaswamy

**Study supervision:** S. Ramaswamy, D. Basu

## Acknowledgments

We thank Christopher Lengner, PhD, for review of this article and the Wistar Flow Cytometry Facility for technical support.

## Grant Support

This work is supported by NIH K08-DE022842 (D. Basu), R21-DE024396 (D. Basu, H. Nakagawa, P. Gimotty, M. Herlyn), R01-CA185086 (S. Ramaswamy), P01-CA098101 (D. Basu, P. Gimotty, H. Nakagawa, A.K. Rustgi), K26-RR032714 (H. Nakagawa), K01-DK103953 and F32-CA174176 (K. Whelan), F32-DE024685 (N. Facompre), P30-DK050306 (Core Facilities), Instituto de Salud Carlos III BA12/00021 (X. Sole), Trio/ACS, VA CPPF awards (D. Basu), and the Abramson Cancer Center core facilities.

The costs of publication of this article were defrayed in part by the payment of page charges. This article must therefore be hereby marked *advertisement* in accordance with 18 U.S.C. Section 1734 solely to indicate this fact.

Received December 15, 2015; revised May 18, 2016; accepted June 15, 2016; published OnlineFirst August 3, 2016.

## References

1. Prince ME, Sivanandan R, Kaczorowski A, Wolf GT, Kaplan MJ, Dalerba P, et al. Identification of a subpopulation of cells with cancer stem cell properties in head and neck squamous cell carcinoma. Proc Natl Acad Sci U S A 2007;104:973–8.
2. Clay MR, Tabor M, Owen JH, Carey TE, Bradford CR, Wolf GT, et al. Single-marker identification of head and neck squamous cell carcinoma cancer stem cells with aldehyde dehydrogenase. Head Neck 2010;32:1195–201.
3. Facompre N, Nakagawa H, Herlyn M, Basu D. Stem-like cells and therapy resistance in squamous cell carcinomas. Adv Pharmacol 2012;65:235–65.
4. Chiou SH, Yu CC, Huang CY, Lin SC, Liu CJ, Tsai TH, et al. Positive correlations of oct-4 and nanog in oral cancer stem-like cells and high-grade oral squamous cell carcinoma. Clin Cancer Res 2008;14:4085–95.
5. Chien CS, Wang ML, Chu PY, Chang YL, Liu WH, Yu CC, et al. Lin28B/let-7 regulates expression of Oct4 and Sox2 and reprograms oral squamous cell carcinoma cells to a stem-like state. Cancer Res 2015;75:2553–65.
6. He Q, Liu Z, Zhao T, Zhao L, Zhou X, Wang A. Bmi1 drives stem-like properties and is associated with migration, invasion, and poor prognosis in tongue squamous cell carcinoma. Int J Biol Sci 2015;11:1–10.
7. Li L, Clevers H. Coexistence of quiescent and active adult stem cells in mammals. Science 2010;327:542–5.
8. Blanpain C, Fuchs E. Epidermal homeostasis: A balancing act of stem cells in the skin. Nat Rev Mol Cell Biol 2009;10:207–17.
9. Deng X, Ewton DZ, Friedman E. Mirk/Dyrk1B maintains the viability of quiescent pancreatic cancer cells by reducing levels of reactive oxygen species. Cancer Res 2009;69:3317–24.
10. Jin K, Ewton DZ, Park S, Hu J, Friedman E. Mirk regulates the exit of colon cancer cells from quiescence. J Biol Chem 2009;284:22916–25.
11. Dey-Guha I, Wolfer A, Yeh AC, Albeck JG, Darp R, Leon E, et al. Asymmetric cancer cell division regulated by AKT. Proc Natl Acad Sci U S A 2011;108:12845–50.
12. Sang L, Roberts JM, Coller HA. Hijacking HES1: How tumors co-opt the anti-differentiation strategies of quiescent cells. Trends Mol Med 2010;16:17–26.
13. Dey-Guha I, Alves CP, Yeh AC, Salony N, Sole X, Darp R, et al. A mechanism for asymmetric cell division resulting in proliferative asynchronicity. Mol Cancer Res 2015;13:223–30.
14. Lechman ER, Gentner B, van Galen P, Giustacchini A, Saini M, Boccalatte FE, et al. Attenuation of miR-126 activity expands HSC *in vivo* without exhaustion. Cell Stem Cell 2012;11:799–811.
15. Ma S, Lee TK, Zheng BJ, Chan KW, Guan XY. CD133+ HCC cancer stem cells confer chemoresistance by preferential expression of the akt/PKB survival pathway. Oncogene 2008;27:1749–58.
16. Kolev VN, Wright QG, Vidal CM, Ring JE, Shapiro IM, Ricono J, et al. PI3K/mTOR dual inhibitor VS-5584 preferentially targets cancer stem cells. Cancer Res 2015;75:446–55.
17. Dubrovska A, Kim S, Salamone RJ, Walker JR, Maira S-M, García-Echeverría C, et al. The role of PTEN/akt/PI3K signaling in the maintenance and viability of prostate cancer stem-like cell populations. Proc Natl Acad Sci U S A 2009;106:268–73.
18. Hardt O, Wild S, Oerlecke I, Hofmann K, Luo S, Wiencek Y, et al. Highly sensitive profiling of CD44+/CD24- breast cancer stem cells by combining global mRNA amplification and next generation sequencing: Evidence for a hyperactive PI3K pathway. Cancer Lett 2012;325:165–74.
19. Roesch A, Vultur A, Bogeski I, Wang H, Zimmermann KM, Speicher D, et al. Overcoming intrinsic multidrug resistance in melanoma by blocking the mitochondrial respiratory chain of slow-cycling JARID1B(high) cells. Cancer Cell 2013;23:811–25.
20. Roesch A, Fukunaga-Kalabis M, Schmidt EC, Zabierowski SE, Brafford PA, Vultur A, et al. A temporarily distinct subpopulation of slow-cycling melanoma cells is required for continuous tumor growth. Cell 2010;141:583–94.
21. Schmitz SU, Albert M, Malatesta M, Morey L, Johansen JV, Bak M, et al. Jarid1b targets genes regulating development and is involved in neural differentiation. EMBO J 2011;30:4586–600.
22. Scibetta AG, Santangelo S, Coleman J, Hall D, Chaplin T, Copier J, et al. Functional analysis of the transcription repressor PLU-1/JARID1B. Mol Cell Biol 2007;27:7220–35.
23. Yamamoto S, Wu Z, Russnes HG, Takagi S, Peluffo G, Vaske C, et al. JARID1B is a luminal lineage-driving oncogene in breast cancer. Cancer Cell 2014;25:762–77.
24. Wang Z, Tang F, Qi G, Yuan S, Zhang G, Tang B, et al. KDM5B is overexpressed in gastric cancer and is required for gastric cancer cell proliferation and metastasis. Am J Cancer Res 2014;5:87–100.
25. Xiang Y, Zhu Z, Han G, Lin H, Xu L, Chen CD, et al. JARID1B is a histone H3 lysine 4 demethylase up-regulated in prostate cancer. Proc Natl Acad Sci U S A 2007;104:19226–31.
26. Lin CS, Lin YC, Adebayo BO, Wu A, Chen JH, Peng YJ, et al. Silencing JARID1B suppresses oncogenicity, stemness and increases radiation sensitivity in human oral carcinoma. Cancer Lett 2015;368:36–45.
27. Cellot S, Hope KJ, Chagraoui J, Sauvageau M, Deneault É, MacRae T, et al. RNAi screen identifies Jarid1b as a major regulator of mouse HSC activity. Blood 2013;122:1545–55.
28. Kuo YT, Liu YL, Adebayo BO, Shih PH, Lee WH, Wang LS, et al. JARID1B expression plays a critical role in chemoresistance and stem cell-like phenotype of neuroblastoma cells. PLoS One 2015;10:e0125343.
29. Stewart MH, Albert M, Sroczynska P, Cruickshank VA, Guo Y, Rossi DJ, et al. The histone demethylase Jarid1b is required for hematopoietic stem cell self-renewal in mice. Blood 2015;125:2075–8.
30. Basu D, Bewley AF, Sperry SM, Montone KT, Gimotty PA, Rasanen K, et al. EGFR inhibition promotes an aggressive invasion pattern mediated by mesenchymal-like tumor cells within squamous cell carcinomas. Mol Cancer Ther 2013;12:2176–86.
31. Roesch A, Mueller AM, Stempfl T, Moehle C, Landthaler M, Vogt T. RBP2-H1/JARID1B is a transcriptional regulator with a tumor suppressive potential in melanoma cells. Int J Cancer 2008;122:1047–57.
32. Kohn AD, Takeuchi F, Roth RA. Akt, a pleckstrin homology domain containing kinase, is activated primarily by phosphorylation. J Biol Chem 1996;271:21920–6.
33. Oyama K, Okawa T, Nakagawa H, Michaylira CZ, Stairs DB, Figueiredo JL, et al. AKT induces senescence in primary esophageal epithelial cells but is permissive for differentiation as revealed in organotypic culture. Oncogene 2007;26:2353–64.
34. Judd NP, Winkler AE, Murillo-Sauca O, Brotman JJ, Law JH, Lewis JSJr, et al. ERK1/2 regulation of CD44 modulates oral cancer aggressiveness. Cancer Res 2012;72:365–74.
35. Feng Z, Puri S, Moudgil T, Wood W, Hoyt CC, Wang C, et al. Multispectral imaging of formalin-fixed tissue predicts ability to generate tumor-infiltrating lymphocytes from melanoma. J Immunother Cancer 2015;3:47.
36. Hu Y, Smyth GK. ELDA: Extreme limiting dilution analysis for comparing depleted and enriched populations in stem cell and other assays. J Immunol Methods 2009;347:70–8.
37. Visus C, Ito D, Amoscato A, Maciejewska-Franczak M, Abdelsalem A, Dhir R, et al. Identification of human aldehyde dehydrogenase 1 family member

A1 as a novel CD8+ T-cell-defined tumor antigen in squamous cell carcinoma of the head and neck. Cancer Res 2007;67:10538–45.
38. Lim E, Wu D, Pal B, Bouras T, Asselin-Labat ML, Vaillant F, et al. Transcriptome analyses of mouse and human mammary cell subpopulations reveal multiple conserved genes and pathways. Breast Cancer Res 2010; 12:R21.
39. Boquest AC, Shahdadfar A, Fronsdal K, Sigurjonsson O, Tunheim SH, Collas P, et al. Isolation and transcription profiling of purified uncultured human stromal stem cells: Alteration of gene expression after *in vitro* cell culture. Mol Biol Cell 2005;16:1131–41.
40. Sarrio D, Rodriguez-Pinilla SM, Hardisson D, Cano A, Moreno-Bueno G, Palacios J. Epithelial-mesenchymal transition in breast cancer relates to the basal-like phenotype. Cancer Res 2008;68:989–97.
41. Gupta PB, Fillmore CM, Jiang G, Shapira SD, Tao K, Kuperwasser C, et al. Stochastic state transitions give rise to phenotypic equilibrium in populations of cancer cells. Cell 2011;146:633–44.
42. Chaffer CL, Marjanovic ND, Lee T, Bell G, Kleer CG, Reinhardt F, et al. Poised chromatin at the ZEB1 promoter enables breast cancer cell plasticity and enhances tumorigenicity. Cell 2013;154:61–74.
43. Kidder BL, Hu G, Yu ZX, Liu C, Zhao K. Extended self-renewal and accelerated reprogramming in the absence of kdm5b. Mol Cell Biol 2013;33:4793–810.
44. Dey BK, Stalker L, Schnerch A, Bhatia M, Taylor-Papidimitriou J, Wynder C. The histone demethylase KDM5b/JARID1b plays a role in cell fate decisions by blocking terminal differentiation. Mol Cell Biol 2008;28:5312–27.
45. Wong PP, Miranda F, Chan KV, Berlato C, Hurst HC, Scibetta AG. Histone demethylase KDM5B collaborates with TFAP2C and myc to repress the cell cycle inhibitor p21(cip) (CDKN1A). Mol Cell Biol 2012;32:1633–44.
46. Zhang Y, Liang J, Li Q. Coordinated regulation of retinoic acid signaling pathway by KDM5B and polycomb repressive complex 2. J Cell Biochem 2014;115:1528–38.
47. Barrett A, Santangelo S, Tan K, Catchpole S, Roberts K, Spencer-Dene B, et al. Breast cancer associated transcriptional repressor PLU-1/JARID1B interacts directly with histone deacetylases. Int J Cancer 2007;121:265–75.
48. Lui VW, Hedberg ML, Li H, Vangara BS, Pendleton K, Zeng Y, et al. Frequent mutation of the PI3K pathway in head and neck cancer defines predictive biomarkers. Cancer Discov 2013;3:761–9.
49. Seiwert TY, Zuo Z, Keck MK, Khattri A, Pedamallu CS, Stricker T, et al. Integrative and comparative genomic analysis of HPV-positive and HPV-negative head and neck squamous cell carcinomas. Clin Cancer Res 2015;21:632–41.
50. Tian H, Biehs B, Warming S, Leong KG, Rangell L, Klein OD, et al. A reserve stem cell population in small intestine renders Lgr5-positive cells dispensable. Nature 2011;478:255–9.